Journal of Sustainable Metallurgy (2022) 8:1498–1508
https://doi.org/10.1007/s40831-022-00617-6

THEMATIC SECTION: REWAS 2022: DEVELOPING TOMORROW'S TECHNICAL CYCLES

Solubilities of RE_2O_3 in REF_3-LiF (RE = Nd, Dy) at 1473 K

Osamu Takeda[1] · Kiyotaka Nakano[1] · Fumiyoshi Kobayashi[1] · Xin Lu[1] · Yuzuru Sato[1] · Hogmin Zhu[1]

Received: 27 March 2022 / Accepted: 16 October 2022 / Published online: 28 October 2022

Abstract

The development of a recycling process for rare-earth-containing waste is important for improving the resource conservation and resource security of rare-earth metals. Phase equilibria between the molten fluoride and rare-earth oxide were investigated to develop a novel recycling process for neodymium magnets based on the flux-remelting method. LiF—rare-earth fluoride (REF_3, RE = Nd, Dy) mixtures and rare-earth oxides (RE_2O_3, RE = Nd, Dy) were selected, and the phase equilibria in the Nd_2O_3–NdF_3–Li_2O–LiF and Dy_2O_3–DyF_3–Li_2O–LiF systems were investigated by differential thermal analysis and chemical equilibrating method. It was revealed that compounds NdOF, $Nd_4O_3F_6$, DyOF, and $Dy_4O_3F_6$ were stable as an equilibrium phase at 1473 K. In the dissolution of Nd_2O_3 in molten LiF–NdF_3, $Nd_4O_3F_6$ formed when the mixing ratio exceeds the solubility limit of the melt and the compound coexists with the melt. In the same manner, $Dy_4O_3F_6$ formed when the mixing ratio exceeds the solubility limit of molten LiF-DyF_3 and the compound coexists with the melt. At 1473 K, the solubilities of Nd_2O_3 in molten LiF—50 mol% NdF_3 and Dy_2O_3 in molten LiF—50 mol% DyF_3 were determined as 7.4 mass% and 7.6 mass%, respectively. An enhancement device for the dissolution rate of oxyfluorides is required for practical applications owing to the slow dissolution rate. The recycling process can be used to regenerate neodymium magnet waste by adding a small amount of virgin rare-earth metals.

Graphical Abstract

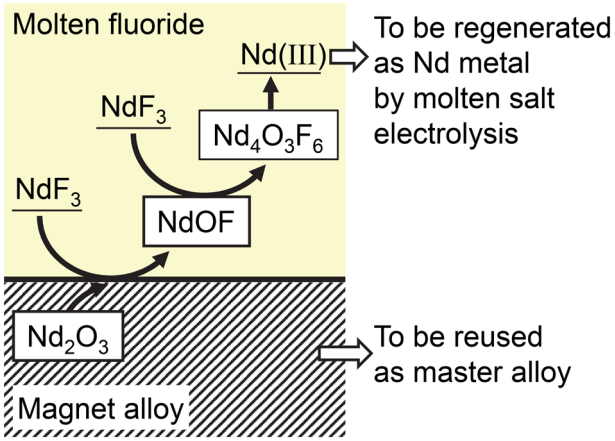

Keywords Rare-earth metal · Recycling · Permanent magnet · Oxide · Fluoride · Oxyfluoride · Solubility

Introduction

Rare earths (RE: Sc, Y, La–Lu) are indispensable for high-performance industrial products, including permanent magnets such as neodymium (Nd) magnets [1, 2]. A rare-earth-sintered magnet, Nd–iron (Fe)–boron (B)-sintered magnet

The contributing editor for this article was Adam Powell.

✉ Osamu Takeda
takeda@material.tohoku.ac.jp

[1] Tohoku University, 6-6-02 Aramaki-Aza-Aoba, Aoba-Ku, Sendai 980-8579, Japan

(Nd magnet), was developed in Japan [1], which is currently one of the largest producers. However, all the raw materials (rare-earth oxides and rare-earth metals) are imported overseas to Japan [3]. In 2010, the import prices of rare-earth metals drastically increased because of a shortage in resource supply [4]. Particularly, the raise of dysprosium (Dy), which is an important additive for increasing coercivity of Nd magnet, was extremely high. Thus, the supply of rare-earth resources is uncertain, and therefore, recycling of rare-earth-containing waste, such as Nd magnet waste, is required to improve resource conservation and resource security of these metals [5–7].

The hydrometallurgical method is the major recycling process for Nd magnet waste [8, 9]. In this process, Nd magnet waste is dissolved in an acid and subjected to solvent extraction for primary resource processing. The hydrometallurgical method has advantages, such as the removal of much impurities and mutual separation of rare-earth elements. However, a large amount of waste solution is generated because, in addition to rare-earth metals, iron, as a major component of the magnet, is dissolved. Furthermore, large amounts of energy are consumed because RE is regenerated to metals via molten salt electrolysis along with raw materials derived from natural ore. Plants with recycling facilities are also few in countries where rare-earth smelters are located, such as China.

Based on the background, novel recycling processes have been developed to recycle Nd magnet waste in Japan. Chemical processes at elevated temperatures (pyrometallurgical recycling processes) developed on a laboratory scale are shown in Fig. 1. Recycling technologies for Nd magnet wastes are classified as (1) "material recycling methods" in which scrap materials are charged into smelting processes as raw material, (2) "alloy recycling methods" in which the materials are regenerated into master alloys for magnet production, and (3) "magnet recycling methods" in which magnet alloys are reused in their current form. For material recycling methods, Murase et al. applied the chemical vapor transport method to extract and separate rare-earth elements from magnet waste by forming complexes of aluminum chloride and rare-earth chlorides (Fig. 1a) [10]. Uda et al. studied the mutual separation of rare-earth halides by utilizing the difference in vapor pressure between rare-earth dihalides and trihalides (Fig. 1b) [11]. The extraction of rare-earth elements from magnet waste was also attempted using a chlorination agent or iodization agent (Fig. 1c, d) [12, 13]. Other roasting methods for rare-earth magnet such as sulfidation [14] and sulfation [15, 16] are also recently explored as other oxidative type methods. In contrast, the extraction of rare-earth metals without oxidation (halogenation) was extensively investigated using molten metals as collector metals (Fig. 1e) [17–24]. The removal of carbon and oxygen in magnet alloy wastes by roasting and calciothermic

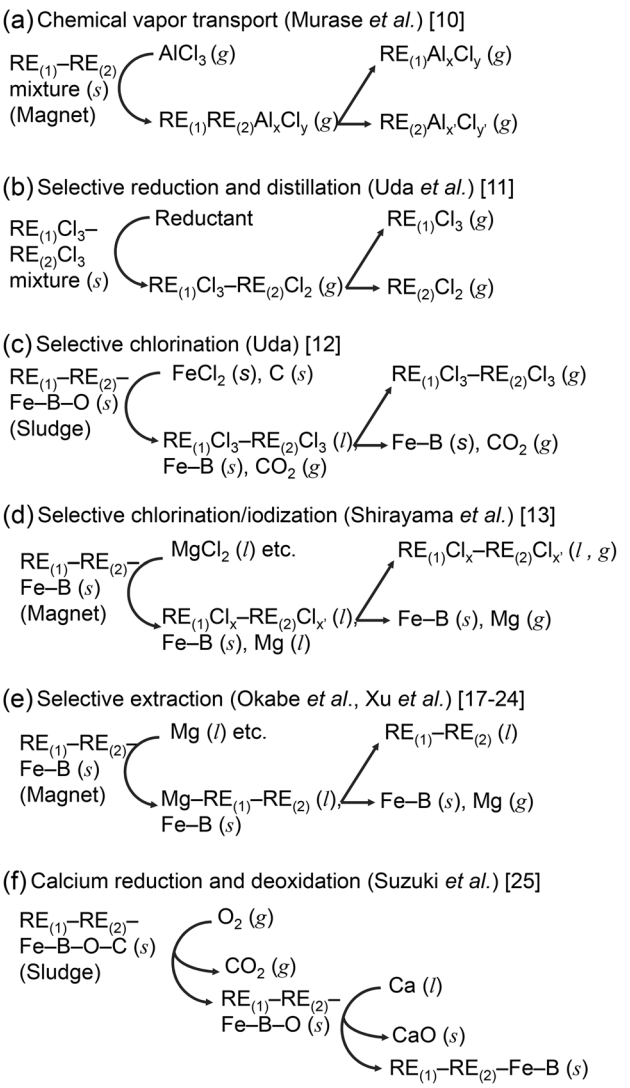

Fig. 1 Pyrometallurgical recycling processes for rare-earth metals developed at the lab scale. [10–25]

reduction/deoxidation was studied as alloy recycling methods (Fig. 1f) [25].

A noteworthy patent proposed the addition of a small amount of fluoride during the remelting of the magnet alloy for smoothly separating the slag and metal [26]. Deoxidation of pure Nd metal using molten fluoride has also been studied [27]. Based on this background, the authors explored a more realistic recycling process for Nd magnet waste and proposed a recycling process to extract rare-earth-oxide inclusions harmful for reproducing magnet alloys from magnet alloy wastes using molten fluoride [28]. The rare-earth-oxide inclusions are mainly located in the boundaries between the grains of matrix phase ($RE_2Fe_{14}B$, RE = Nd, Pr, Dy) [28]. The matrix has to be decomposed in order to liberate the inclusions. A schematic of the extraction process is presented in Fig. 2.

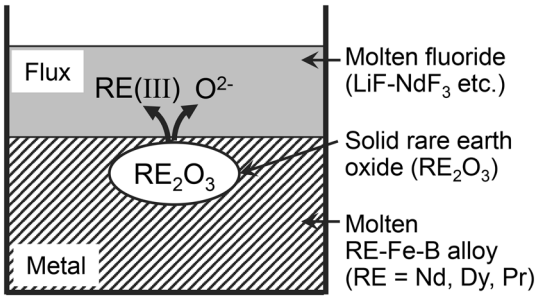

Fig. 2 Schematic of the refining process for extracting the rare-earth oxide present in magnet waste using molten fluoride

In this process, Nd magnet alloys containing rare-earth oxides are remelted together with fluoride flux. The oxides rise in the molten alloy to dissolve into the molten fluoride. The refined alloys are used as the master alloys for magnet production. The separated oxides are reduced to metals by conventional molten salt electrolysis in molten fluoride. After electrolysis, the fluoride is circulated for the extraction process. The recycling process is highly feasible from an industrial point of view because (1) the reactor is simple; (2) the liquid–liquid separation (molten fluoride/molten alloy) is suitable for large-scale treatment; (3) the energy consumption is low because most of the alloy is regenerated without oxidation; and (4) no waste solution is generated.

The most important property of the fluoride flux in the extraction process is the solubility of rare-earth oxides in the molten fluoride. However, the solubility data at high temperatures are limited. For instance, it was reported that the solubilities of cerium oxide (CeO_2) into a molten cerium fluoride (CeF_3)—12 mass% barium fluoride (BaF_2)—15 mass% lithium fluoride (LiF) were 1.7 and 2.1 mass% at 1073 and 1123 K, respectively [29]. Similarly, the solubility of lanthanum oxide (La_2O_3) into a molten lanthanum fluoride (LaF_3)—27 mass% LiF—13 mass% BaF_2 was approximately 2.5 mass% at 1223 K [29]. There are no systematic reports on the solubility of Nd_2O_3 and Dy_2O_3 in molten fluoride.

In this study, the phase equilibria between molten fluoride and Nd_2O_3 and Dy_2O_3 were investigated to determine their solubilities. A mixture of LiF and REF_3 (RE = Nd, Dy) was selected as the fluoride. RE_2O_3 is known to react with REF_3 to form chemically stable oxyfluorides (REOF and $RE_4O_3F_6$) [30, 31]. However, the phase stabilities of REOF and $RE_4O_3F_6$ at high temperatures remain unclear. Therefore, phase stabilities were analyzed using differential thermal analysis (DTA). The phase equilibria of the systems containing REOF and $RE_4O_3F_6$ were studied using the chemical equilibrating method. These results were used to investigate the dissolution process of rare-earth oxides into molten fluoride.

The proposed process [28] requires operating temperatures that are higher than the peritectic point of $Nd_2Fe_{14}B$ (1454 K [32]), which is the major phase of the Nd magnet, to efficiently extract rare-earth oxides. Heating the Nd magnet alloy above the peritectic temperature decomposes solid $Nd_2Fe_{14}B$ into solid γ-Fe and liquid Nd–Fe–B phases, and the rare-earth oxide present in the alloy is liberated. Therefore, the experimental temperature was set at 1473 K (1200 °C), which is higher than the peritectic point of $Nd_2Fe_{14}B$.

Experimental

Sample Preparation

Reagent powders of Nd_2O_3 (99.9% purity, Soekawa Chemical Co. Ltd) and Dy_2O_3 (99.9% purity, Kojundo Chemical Laboratory Co. Ltd.) were pressed at 6 MPa to form pellets. These were stacked on an alumina plate, heated, and maintained at 1773 K for 3 h in air to transform a small amount of rare-earth hydrocarbonates contained in the reagents to rare-earth oxides by roasting. After cooling, the pellets were crushed, pulverized, and subjected to equilibrating experiments and oxyfluoride synthesis. Nd oxyfluorides were synthesized by pressing a mixture of Nd_2O_3 and NdF_3 at 6 MPa to form pellets. The pellets were heated at 1173 K for 10 h under vacuum to synthesize NdOF and $Nd_4O_3F_6$ according to reactions (1) and (2).

$$Nd_2O_3 + NdF_3 = 3\,NdOF, \tag{1}$$

$$Nd_2O_3 + 2\,NdF_3 = Nd_4O_3F_6. \tag{2}$$

The above conditions for the synthesis of oxyfluorides were set according to the previous study [33]. DyOF and $Dy_4O_3F_6$ were synthesized in the same manner.

Reagent powders of LiF (98% purity, Kanto Chemical Co., Inc.) and neodymium fluoride (NdF_3, 99.9% purity, Nippon Yttrium Co. Ltd.) were mechanically mixed to obtain LiF-*x* mol% NdF_3 ($x = 25, 50$) as the fluoride flux. Similarly, reagent powders of LiF and dysprosium fluoride (DyF_3, 99.9% purity, Nippon Yttrium Co. Ltd.) were mixed to obtain LiF-*x* mol% DyF_3 ($x = 25, 50$). The mixed salts were placed in an iron crucible (99.7% purity) and hermetically sealed using tungsten inert gas (TIG) welding. The mixed salts were then heated and melted at 1473 K for 3 h. After cooling, the salts were crushed and pulverized for subsequent experiments.

Experimental Procedure

Phase Stability Analysis

DTA experiments were conducted with 10 to 20 mg of synthesized oxyfluorides (NdOF, $Nd_4O_3F_6$, DyOF, and

$Dy_4O_3F_6$) placed in an alumina pan, using a thermal analysis instrument (SDT Q600, TA instruments, USA). The temperature was increased from 293 to 1523 K (50 K higher than 1473 K as the target temperature) at a heating rate of 5 K·min^{-1} under an argon flow of 100 mL·min^{-1}. The reference material was alumina powder (99.9% purity).

Determination of Phase Equilibria and Dissolution Investigations

Schematic representations of the vessel containing the samples and of the entire experimental apparatus, including the electric furnace, are shown in Fig. 3. The pre-determined compositions of the mixed samples were plotted as a reciprocal system in a compositional square (Fig. 4).

For Exp. A to J for the Nd system (LiF−NdF_3/Nd_2O_3), and Exp. Q to S for the Dy system (LiF−DyF_3/Dy_2O_3), mixed fluoride powders (0.316−6.859 g) and oxide powders (0.300–0.937 g) were well mixed and placed in an iron crucible to determine phase equilibria. For Exp. K to O for the Nd system (LiF−NdF_3/NdOF), and Exp. U to X for the Dy system (LiF−DyF_3/DyOF), oxyfluoride pellets were placed in an iron crucible, and the mixed fluoride powders were placed on the pellets to determine the phase equilibria and solubility.

In the neodymium system in the compositional square (Fig. 4a), Exp. A has the highest oxide concentration (lowest fluoride concentration), and Exp. M has the lowest oxide concentration (highest fluoride concentration). In the dysprosium system in the compositional square (Fig. 4b), Exp. Q has the highest oxide concentration, whereas Exp. W exhibits the lowest oxide concentration.

The mixed samples were placed in an iron crucible (99.7% purity, diameter and depth of 10 mm) and sealed using TIG welding. Three to four crucibles containing

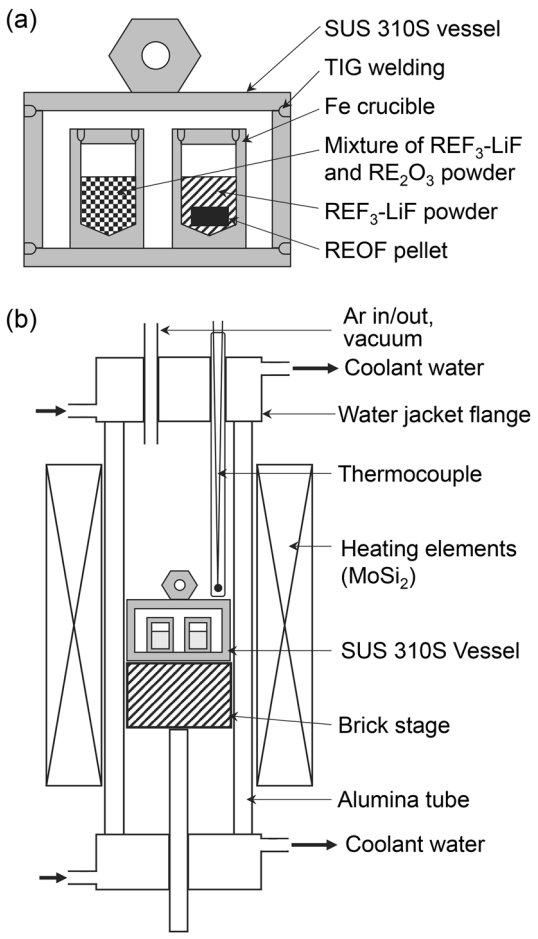

Fig. 3 Schematic illustration of **a** the vessel containing the samples and **b** entire experimental apparatus including an electric furnace

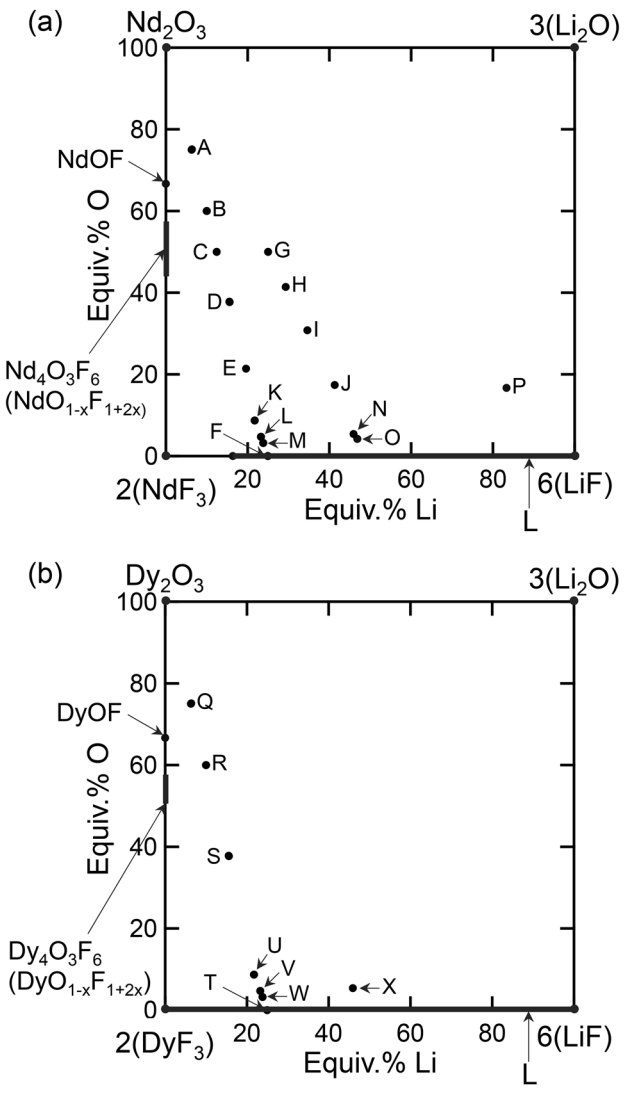

Fig. 4 Compositions of the mixed samples for determining the phase equilibria of the **a** LiF−NdF_3−Li_2O−Nd_2O_3 and **b** LiF−DyF_3−Li_2O−Dy_2O_3 systems

samples of different compositions were placed in a stainless-steel (SUS 310S in JIS standard) container that was sealed using TIG welding. The container was placed in a high-purity alumina tube in an electric furnace and heated at 1473 K for 86.4−605 ks (24–168 h). After the experiment, the container was removed from the alumina tube and quenched with water (The quench rate was estimated as approximately 130 $K \cdot s^{-1}$ on average). The recovered crucible was cut into two pieces, and the cross section was visually observed. A piece mounted in a resin was polished using emery papers, and a diamond paste (under 1 μm diameter particle) was observed using a scanning electron microscope with an energy-dispersive X-ray spectrometer (SEM–EDX, XL-30FEG, Philips Co.). The salt sample contained in another piece was mechanically peeled, crushed, and pulverized for X-ray diffraction analysis (XRD, Ultima IV, Rigaku Co.).

Results and Discussion

Phase Stability of Oxyfluorides up to 1473 K

The XRD patterns of synthesized Nd_2O_3, NdOF, and $Nd_4O_3F_6$ are shown in Fig. 5. The XRD patterns were consistent with powder diffraction data files edited by International center for diffraction data (ICDD). The color of Nd_2O_3 was navy, while that of NdOF and $Nd_4O_3F_6$ was aqua. Nd oxide and oxyfluorides were easily distinguished from the fluoride because the color of the mixed fluoride was white. DyOF and $Dy_4O_3F_6$ were synthesized in the same manner. It was difficult to visually distinguish Dy_2O_3, DyOF, and $Dy_4O_3F_6$ from mixed fluoride because all the compounds were white.

The DTA curves for analyzing the phase stability of the rare-earth oxyfluorides are shown in Fig. 6. NdOF undergoes an endothermic phase transformation at 797 K, which is attributed to the transformation from rhombohedral to cubic crystals [30]. The transformation temperature was close to that reported in the literature (788 K [30] and 800 K [34]). No transformation was observed between the transformation temperature and 1473 K, indicating the stability of solid NdOF at 1473 K. This agrees with the report by Niihara and Yajima [30].

$Nd_4O_3F_6$ exhibited no phase transformation from 293 to 1473 K, which is consistent with some previous reports [30, 35]. $Nd_4O_3F_6$ was also stable as a solid at 1473 K.

DyOF underwent an endothermic phase transformation at 831 K (transformation from rhombohedral to cubic crystals [30]). The transformation temperature was slightly lower than those reported in the literature (852 K [30], 842 K [34]). No further transformation was observed above the

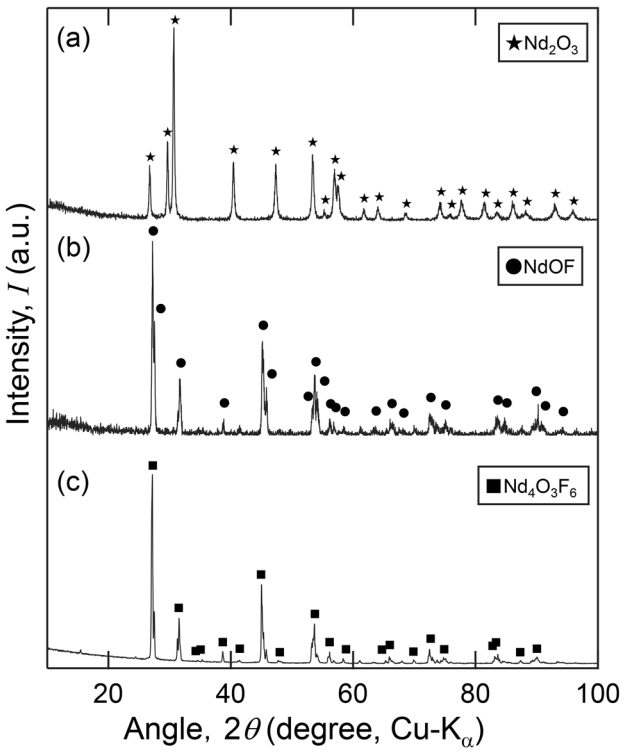

Fig. 5 X-ray diffraction patterns of **a** roasted Nd_2O_3, **b** synthesized NdOF, and **c** synthesized $Nd_4O_3F_6$. Reference pattern No. in JCPDS; Nd_2O_3: 43–1023, NdOF: 17–276, $Nd_4O_3F_6$: 01–070-5458

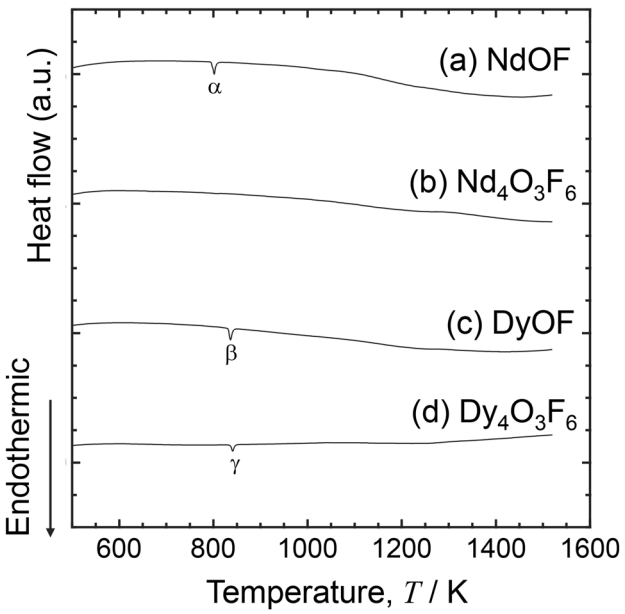

Fig. 6 DTA curves for analyzing the phase stability of rare-earth oxyfluorides (5 $K \cdot min^{-1}$). **a** NdOF, **b** $Nd_4O_3F_6$, **c** DyOF, (*d*) $Dy_4O_3F_6$. Peaks α and β: rhombohedral to cubic transition. Peak γ: tetragonal to unknown crystal transition

transformation temperature, which indicates that DyOF is stable as a solid at 1473 K.

$Dy_4O_3F_6$ exhibited a phase transformation at 843 K, which exhibits a considerable discrepancy with the results obtained by Niihara and Yajima [30], who observed a transformation from tetragonal to unknown crystals at 1322 K. Kozak et al. [36] reported the decomposition of $Dy_4O_3F_6$ to DyOF and $Dy_{1+x}O_{3x}F_{3(1-x)}$ at 1348 K; however, evidence of decomposition was not observed in the present study. Because an endotherm corresponding to melting was not detected during the DTA experiment and no change in the morphology of the $Dy_4O_3F_6$ sample by melting was observed after the DTA experiment, it was concluded that $Dy_4O_3F_6$ is stable as a solid at 1473 K.

Phase Equilibria Determination of the RE_2O_3-REF_3-LiF system (RE = Nd, Dy)

The XRD patterns of the samples containing Nd_2O_3 mixed with LiF—50 mol% NdF_3 and Nd_2O_3 mixed with LiF—25 mol% NdF_3 are shown in Figs. 7 and 8, respectively. Nd_2O_3 disappeared, and NdOF was formed with decreasing oxide concentration (Exps. A to F/Exp. G to J). Then, NdOF disappeared and $Nd_4O_3F_6$ was formed as the oxide concentration decreased further. It has been reported that $Nd_4O_3F_6$ forms a solid solution, as indicated by the formula $NdO_{1-x}F_{1+2x}$ ($x = 0.15$–0.34) [31], but the difference in composition could not be identified in the present study because analytical precision of SEM–EDX on gas elements such as oxygen and fluorine are very low. Nd oxide was found to be converted in the order of NdOF and $Nd_4O_3F_6$. It was estimated that $Nd_4O_3F_6$ dissolved into the molten fluoride to form ionic species.

Pure Nd_2O_3 and pure LiF were mixed in Exp. P. Nd_2O_3 and pure LiF were observed after the experiment. It was confirmed that the following reaction did not occur, and Nd_2O_3 equilibrated with LiF.

$$Nd_2O_3 + 6\,LiF = 2\,NdF_3 + 3Li_2O. \quad (3)$$

It is reasonable to investigate the equilibria in the composition triangle comprising Nd_2O_3, NdF_3, and LiF corners in this study.

The XRD patterns of the sample containing Dy_2O_3 mixed with LiF—50 mol% DyF_3 are shown in Fig. 9. The oxide concentration decreases from Exp. Q to R. The compound $LiDyF_4$, identified in Exp. T, is by a peritectic reaction (peritectic point: 1137 K) during the cooling of the sample after the experiment. Dy_2O_3 disappeared, and DyOF was formed by decreasing the oxide concentration. Subsequently, DyOF disappeared, and $Dy_4O_3F_6$ was formed as the oxide concentration decreased further. Thus, dysprosium oxide was converted in the order of DyOF and $Dy_4O_3F_6$. It was considered that $Dy_4O_3F_6$ dissolved into the molten fluoride to form ionic species. Based on the above results, it was considered that rare-earth oxides dissolve into molten fluoride by forming several rare-earth oxyfluorides.

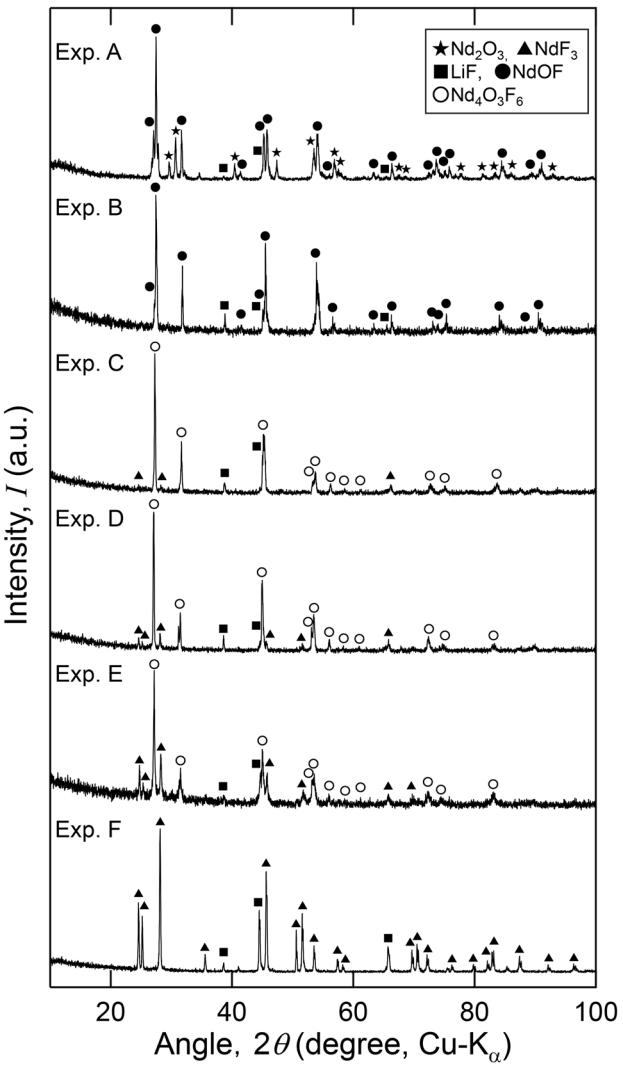

Fig. 7 X-ray diffraction patterns of the samples obtained after the equilibrium experiments A to F at 1473 K for 24 h. Reference pattern No. in JCPDS; Nd_2O_3: 43–1023, NdF_3: 9–416, LiF: 4–857, NdOF: 17–276, $Nd_4O_3F_6$: 50–635

Solubility and Dissolution Process of Oxyfluoride in Molten Fluoride

Figure 10 shows the photographic and SEM images of the iron crucible's cross section after the experiment in which the NdOF pellet was mixed with molten LiF—50 mol% NdF_3 at 1473 K. The mixing ratio (R_M) is defined as follows:

$$R_M = n_{LiF-NdF3}/n_{NdOF}, \quad (4)$$

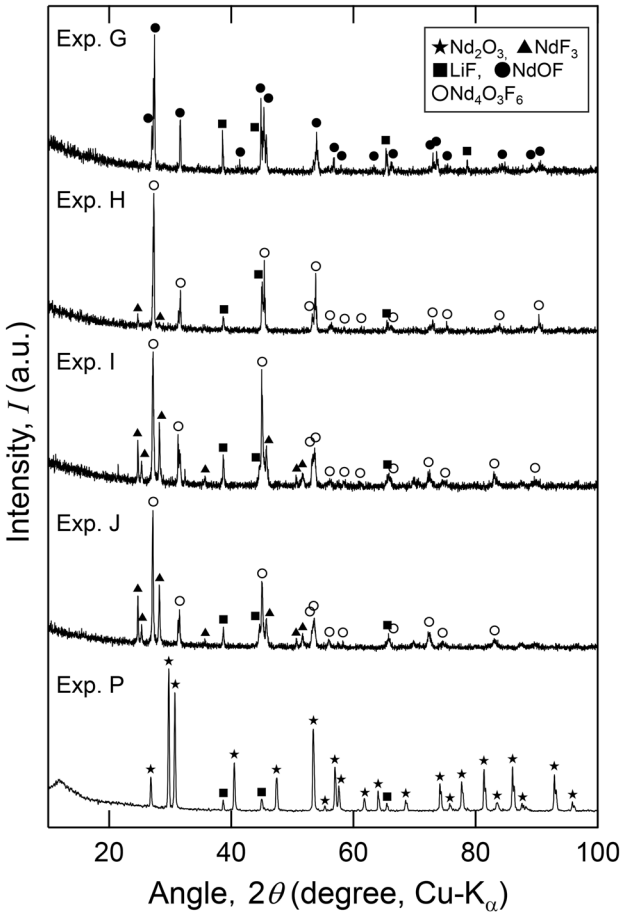

Fig. 8 X-ray diffraction patterns of the samples obtained after the equilibrium experiments G, H, I, J, and P. at 1473 K for 24 h. Reference pattern No. in JCPDS; Nd_2O_3: 43–1023, NdF_3: 9–416, LiF: 4–857, NdOF: 17–276, $Nd_4O_3F_6$: 50–635

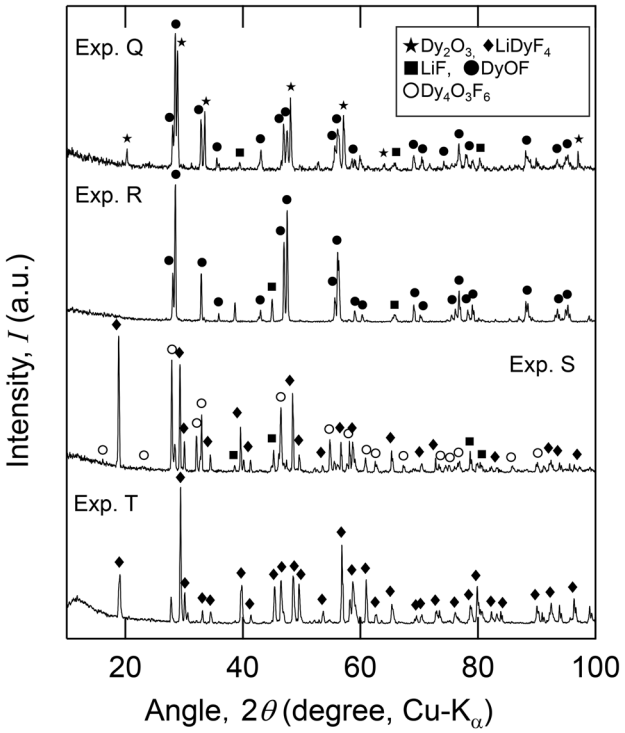

Fig. 9 X-ray diffraction patterns of the samples obtained after the equilibrium experiments Q, R, S, and T at 1473 K for 24 h. Reference pattern No. in JCPDS; Dy_2O_3: 43–1006, $LiDyF_4$: 27–1233, LiF: 4–857, DyOF: 19–437, $Dy_4O_3F_6$: 33–523

where $n_{\text{LiF-NdF3}}$ and n_{NdOF} represent the number of moles of fluoride (based on the average formula weight) and NdOF, respectively. The R_M for the experiments shown in Fig. 10 was 20. A residue was visually observed at the bottom of the crucible after 24 h of holding. SEM–EDX revealed that the bulky particles in the residue were undissolved oxyfluoride (NdO_xF_y). Fine particles of oxyfluoride (NdO_xF_y) precipitated in the supernatant (flux region) during quenching were also observed. No residue was observed at the bottom of the crucible over 72 h, either visually or microscopically.

The experimental results obtained by mixing NdOF to LiF—50 mol% NdF_3 are summarized in Fig. 11. The horizontal and vertical axes indicate the holding time and mixing ratio R_M, respectively. When R_M was 10, residues were observed after 24, 72, and 168 h. Therefore, the fluoride was saturated by neodymium oxyfluoride. When the values of R_M were 20 and 30, the residue disappeared after 72 h of holding. Thus, the concentrations of oxyfluoride in the fluorides were lower than the solubility.

Based on the results, it was determined that the solubility of NdOF in molten LiF—50 mol% NdF_3 at 1473 K was 7.9 mass%. The solubility of Nd_2O_3 in the molten salt was converted 7.4 mass%. Similarly, it was determined that the solubility of DyOF in molten LiF—50 mol% DyF_3 at 1473 K was 8.0 mass%. The solubility of Dy_2O_3 in the molten salt was converted 7.6 mass%. Therefore, both the solubilities were similar.

The SEM images of the residue and precipitates after the dissolution of NdOF into molten LiF—50 mol% NdF_3 and molten LiF—25 mol% NdF_3 are shown in Fig. 12. For molten LiF—50 mol% NdF_3, many fine particles of oxyfluoride precipitated during solidification were observed in the flux region, whereas particles of oxyfluoride were hardly observed in the flux region for molten LiF—25 mol% NdF_3.

From the viewpoint of kinetics, it took a time over 24 h for complete dissolution of NdOF into molten fluoride. This means that dissolution rate of oxyfluoride into molten fluoride is very slow because the experiments were carried out without stirring. Therefore, an enhancement device for the dissolution rate, such as agitation of the melt, is required for practical applications to perform the extraction process efficiently.

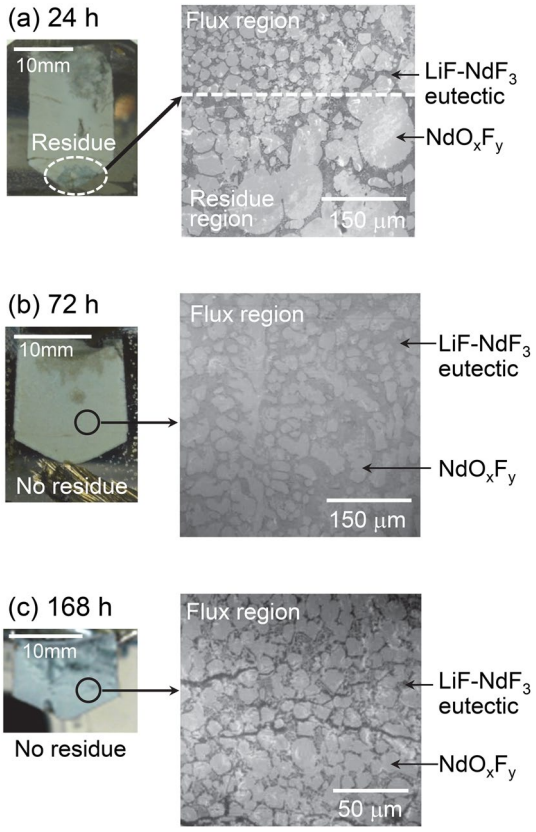

Fig. 10 Photographs (left) and SEM images (right) of the cross section of the Fe crucible after the experiment for determining the solubility of NdOF in molten LiF—50 mol% NdF_3 system [Exp. L]. Holding time; **a** 24 h, **b** 72 h, **c** 168 h

Phase Diagram for the RE_2O_3–REF_3–LiF System (RE = Nd, Dy)

The partial phase diagram for the Nd_2O_3–NdF_3–Li_2O–LiF system at 1473 K, constructed based on the above discussion, is shown in Fig. 13a. The horizontal and vertical axes indicate equivalent concentrations of lithium and oxygen, respectively. The composition regions surrounded by Nd_2O_3 (*s*)/LiF (*l*)/Li_2O (*s*) and $Nd_4O_3F_6$ (*s*)/NdF_3 (*s*)/NdF_3–LiF (*l*) were not investigated. Ternary phase equilibrium of Nd_2O_3 (*s*)/NdOF (*s*)/LiF (*l*) in the Nd_2O_3-rich region, and another ternary phase equilibrium of NdOF (*s*)/$Nd_4O_3F_6$ (*s*)/LiF (*l*) is established by lowering the Nd_2O_3 concentration. The binary phase equilibria of $Nd_4O_3F_6$ (*s*)/NdF_3–LiF (*l*) appear with a further decrease in the Nd_2O_3 concentration. Solubility width of $Nd_4O_3F_6$ was drawn along the literature [31]. Tie lines (dashed line) were drawn by an estimation along the phase rule. At a high temperature of 1473 K, any components in the system studied must have mutual solubilities to some extent. For instance, LiF must have a certain level of solubility of Nd_2O_3. However, the mutual solubilities are ignored in the present study because of lack of solubility data. In order to construct more accurate phase diagram, the solubility data have to be obtained. For example, it may be effective that molten LiF saturated with Nd_2O_3 at 1473 K is sampled and Nd and O concentrations in the LiF are measured. We will continue to work on the task to construct more accurate phase diagram. The hatched region in the diagram exhibits a homogeneous liquid phase. A homogeneous liquid phase should be formed during the practical extraction process by adding sufficient fluoride flux.

The partial phase diagram for the Dy_2O_3–DyF_3–Li_2O–LiF system at 1473 K is shown in Fig. 13b. The composition regions surrounded by Dy_2O_3 (*s*)/LiF (*l*)/Li_2O (*s*) were excluded for the same reason as in the case of the neodymium system. A ternary phase equilibrium of Dy_2O_3 (*s*)/DyOF (*s*)/LiF (*l*) is observed in the Dy_2O_3-rich region, and another ternary phase equilibrium of DyOF (*s*)/$Dy_4O_3F_6$ (*s*)/LiF (*l*) is established by decreasing the Dy_2O_3 concentration. The binary phase equilibria of $D_4O_3F_6$ (*s*)/DyF_3–LiF (*l*) appear with a further decrease in the Dy_2O_3 concentration. Solubility width of $Dy_4O_3F_6$ was drawn along the literature [36]. Tie lines (dashed line) were drawn by an estimation along the phase rule. In the same manner with the system containing neodymium, the mutual solubilities between involved components are ignored in the system containing dysprosium because of lack of solubility data. In order to construct more accurate phase diagram, we will continue to work on the solubility measurement at high temperatures. It is estimated that $Dy_4O_3F_6$ (*s*) equilibrates with molten fluorides containing oxyfluoride ions. The homogeneous liquid phase shown in the hatched region should be produced during a practical extraction process by adding sufficient fluoride flux in the same manner as the neodymium system.

Future Prospects for Practical Application

Figure 14 shows a schematic illustration of the extraction process of rare-earth oxides from a magnet alloy using molten fluoride. Nd_2O_3 in the alloy reacts with NdF_3 in molten fluoride to form NdOF, which successively reacts with NdF_3 to form $Nd_4O_3F_6$. $Nd_4O_3F_6$ finally dissolves in molten fluoride to form an oxyfluoride ion.

A Nd-sintered magnet generally contains approximately 31 mass% of rare-earth metals (Nd + Pr + Dy) and approximately 0.5 mass% of oxygen [25]; for instance, 100 kg of magnet alloy contains 31 kg of rare-earth metals and 0.5 kg of oxygen. If oxygen exists as Nd_2O_3, 100 kg of magnet alloy contains approximately 3.5 kg of Nd_2O_3. Based on the solubility of Nd_2O_3 (7.4 mass%) in LiF—50 mol% NdF_3 at 1473 K, approximately 47 kg of flux is required to completely dissolve Nd_2O_3. Therefore, a considerable amount of flux is required. However, the flux can be reused several times after regenerating rare-earth metals using molten salt electrolysis. The loss of rare-earth metals from magnet

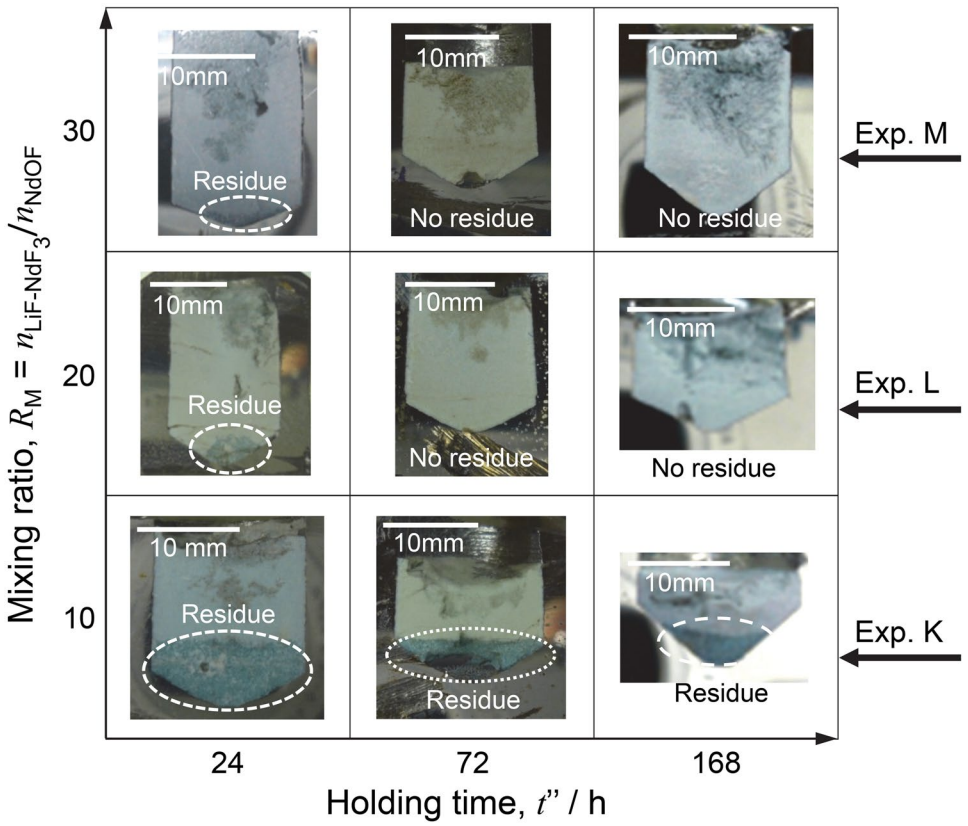

Fig. 11 Photographs of the Fe crucible's cross section after the experiments for determining the solubility of NdOF in molten LiF—50 mol% NdF_3 system [Exps. K, L, and M]

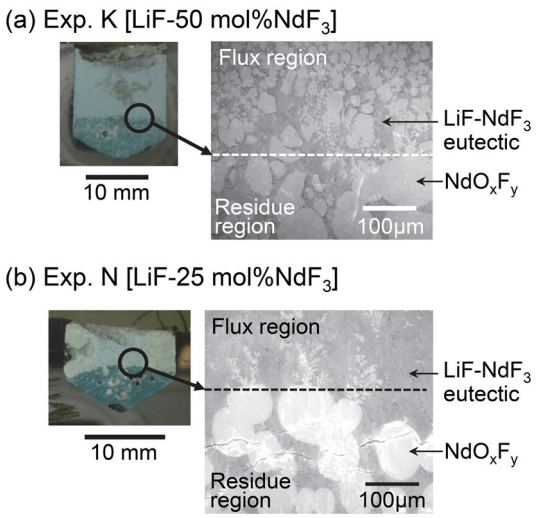

Fig. 12 Photographs (left) and SEM images (right) of the Fe crucible's cross section after the experiments for determining the solubility of NdOF **a** in molten LiF—50 mol% NdF_3 system [Exp. K] and **b** in molten LiF—25 mol% NdF_3 system [Exp. N]. Holding time: 24 h

alloys after refining is approximately 10%. Virgin metals corresponding to the lost rare-earth metals must be added for regenerating magnet alloys. In other words, magnetic waste can be regenerated with a small amount of virgin metals. The materials and energy required for recycling are extremely low compared to the current recycling process based on hydrometallurgical method.

Conclusions

The phase equilibria between molten fluoride and rare-earth oxide were investigated to develop a recycling process for Nd magnets using molten fluoride. LiF–REF_3 and RE_2O_3 (RE = Nd, Dy) were selected as the fluoride and oxide, respectively. In the dissolution of Nd_2O_3 in molten LiF-NdF_3, $Nd_4O_3F_6$ formed when the mixing ratio exceeds the solubility limit of the melt and the compound coexists with the melt. In the same manner, $Dy_4O_3F_6$ formed when the mixing ratio exceeds the solubility limit of molten

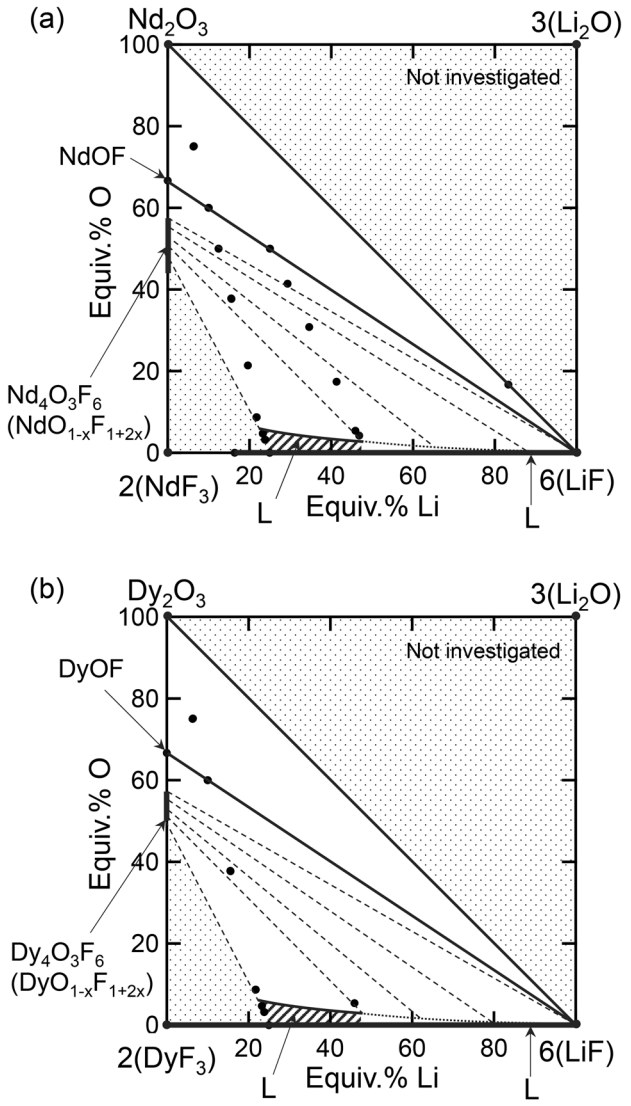

Fig. 13 Determined phase diagrams for the **a** LiF–NdF_3–Li_2O–Nd_2O_3 and **b** LiF–DyF_3–Li_2O–Dy_2O_3 systems at 1473 K. The black dots indicate the composition of the mixed samples

LiF-DyF_3 and the compound coexists with the melt. At 1473 K, the solubility of Nd_2O_3 in LiF—50 mol% NdF_3 was determined as 7.4 mass%, while that of Dy_2O_3 in LiF—50 mol% DyF_3 was determined as 7.6 mass%. An enhancement device for the dissolution rate, such as agitation of the melt, is required for practical applications. Partial phase diagrams in Nd_2O_3–NdF_3–Li_2O–LiF and Dy_2O_3–DyF_3–Li_2O–LiF systems were constructed, and a homogeneous liquid region suitable for efficient extraction was revealed. The recycling process developed in this study can be used to regenerate Nd magnet waste by adding a small amount of virgin metals.

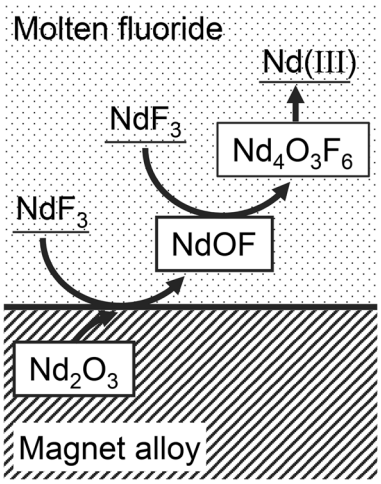

Fig. 14 Estimated steps during the dissolution of Nd_2O_3 into molten fluoride

Acknowledgements This work was financially supported by a Grant-in-Aid for Young Scientists (Start-up) (Project ID No. 19860015) and by a Scientific Research (S) (Project ID No. 19H05623) from the Ministry of Education, Culture, Sports, Science, and Technology (MEXT), Japan, and Research Grant from the Arai Science and Technology Foundation.

Declarations

Conflict of interest On behalf of all authors, the corresponding author states that there is no conflict of interest.

References

1. Sagawa M, Sagawa M, Fujimura S, Togawa N, Yamamoto H, Matsuura Y (1984) New material for permanent magnets on a base of Nd and Fe (invited). J Appl Phys 55:2083–2087
2. Croat JJ, Croat JJ, Herbst JF, Lee RW, Pinkerton FE (1984) Pr-Fe and Nd-Fe-based materials: a new class of high-performance permanent magnets (invited). J Appl Phys 55:2078–2082
3. Yoshida N (2006) Resource of rare earths: an overview of functions and applications of rare earths. In: Adachi G (ed) Resource of rare earths: an overview of functions and applications of rare earths. CMC Publishing, Tokyo, pp 1–6 (**in Japanese**)
4. Takeda O, Lu X, Zhu H (2022) Recent trend on the studies of recycling technologies of rare earth metals. In: REWAS 2022: Developing Tomorrow's Technical Cycles (Volume I), The Minerals, Metals & Materials Series, USA, pp. 259–266
5. Takeda O, Okabe TH (2014) Current status on resource and recycling technology for rare earths. Metall Mater Trans E 1A:160–173
6. Tanaka M, Oki T, Koyama K, Narita H, Oishi T (2013) Recycling of rare earths from scrap. Handb Phys Chem Rare Earths 43:159–211
7. Binnemans K, Jones PT, Blanpain B, Gerven TV, Yang Y, Walton A, Buchert M (2013) Recycling of rare earths: a critical review. J Cleaner Prod 51:1–22
8. Ishigaki N, Ohta A (2006) Recycling technology: an overview of functions and applications of rare earths. In: Adachi G (ed)

Recycling technology: an overview of functions and applications of rare earths. CMC Publishing, Tokyo, pp 13–16 (**in Japanese**)
9. Nakamura E (2006) Alternate materials and recycling of rare metals. In: Harada K (ed) Alternate materials and recycling of rare metals. CMC Publications, Tokyo, pp 296–304 (**in Japanese**)
10. Murase K, Machida K, Adachi G (1995) Recovery of rare metals from scrap of rare earth intermetallic material by chemical vapour transport. J Alloys Compd 217:218–225
11. Uda T, Jacob KT, Hirasawa M (2000) Technique for enhanced rare earth separation. Science 289:2326–2329
12. Uda T (2002) Recovery of rare earths from magnet sludge by $FeCl_2$. Mater Trans 43:55–62
13. Shirayama S, Okabe TH (2018) Selective extraction and recovery of Nd and Dy from Nd-Fe-B magnet scrap by utilizing molten $MgCl_2$. Metall Mater Trans B 49B:1067–1078
14. Stinn C, Allanore A (2021) Selective sulfidation of metal compounds. Nature 602:78–83
15. Carlson BN, Taylor PR (2017) Selective sulfation roasting of rare earths from NdFeB magnet scrap. In: Carlson BN, Taylor PR (eds) Applications of process engineering principles in materials processing, energy and environmental technologies. Springer, Berlin, pp 293–299
16. Önal MAR, Borra CR, Guo M, Blanpain B, Van Gerven T (2015) Recycling of NdFeB magnets using sulfation, selective roasting, and water leaching. J Sustain Metall 1:199–215
17. Xu Y, Chumbley LS, Laabs FC (2000) Liquid metal extraction of Nd from NdFeB magnet scrap. J Mater Res 15:2296–2304
18. Okabe TH, Takeda O, Fukuda K, Umetsu Y (2003) Direct extraction and recovery of neodymium metal from magnet scrap. Mater Trans 44:798–801
19. Takeda O, Okabe TH, Umetsu Y (2004) Phase equilibrium of the system Ag–Fe–Nd, and Nd extraction from magnet scraps using molten silver. J Alloys Compd 379:305–313
20. Takeda O, Okabe TH, Umetsu Y (2005) Phase equilibria of the system Fe–Mg–Nd at 1076 K. J Alloys Compd 392:206–213
21. Takeda O, Okabe TH, Umetsu Y (2006) Recovery of neodymium from a mixture of magnet scrap and other Scrap. J Alloys Compd 408–412:387–390
22. Chae HJ, Kim YD, Kim BS, Kim JG, Kim T (2014) Experimental investigation of diffusion behavior between molten Mg and Nd-Fe-B magnets. J Alloys Compd 586:S143–S149
23. Moore M, Gebert A, Stoica M, Uhlemann M, Löser W (2015) A route for recycling Nd from Nd-Fe-B magnets using Cu melts. J Alloys Compd 647:997–1006
24. Akahori T, Miyamoto Y, Saeki T, Okamoto M, Okabe TH (2017) Optimum conditions for extracting rare earth metals from waste magnets by using molten magnesium. J Alloys Compd 703:337–343
25. Asabe K, Saguchi A, Takahashi W, Suzuki RO, Ono K (2001) Recycling of rare earth magnet scraps: part I, carbon removal by high temperature oxidation. Mater Trans 42:2487–2491
26. Hirota K, Minowa T (2003) Remelting method of rare earth magnet scrap and/or sludge for magnet alloy and rare earth sintered magnet. Japanese Patent A, No. 2003-113429
27. Sano H, Tashiro M, Fujisawa T, Yamauchi C (1999) Deoxidation of neodymium by halide flux treatment. Mater Trans 40:263–267
28. Takeda O, Nakano K, Sato Y (2014) Recycling of rare earth magnet waste by removing rare earth oxide with molten fluoride. Mater Trans 55:334–341
29. Porter B, Brown EA (1961) Determination of oxide solubility in molten fluorides. U.S. Bur. Mines Rep. Invest., No. 5878
30. Niihara K, Yajima S (1972) Studies of rare earth oxyfluorides in the high-temperature region. Bull Chem Soc Jpn 45:20–23
31. Fergus JW (1996) Crystal chemistry of neodymium oxyfluoride. Mater Res Bull 31:1317–1323
32. Hallemans B, Wollants P, Roos JR (1995) Thermodynamic assessment of the Fe-Nd-B phase diagram. J Phase Equilib 16:137–149
33. Niihara K, Yajima S (1971) The crystal structure and nonstoichiometry of rare earth oxyfluoride. Bull Chem Soc Jpn 44:643–648
34. Petzel T, Marx V, Hormann B (1993) Thermodynamics of the rhombohedral-cubic phase transition of ROF R≡ Y, La, Pr, Nd, Sm-Er. J Alloys Compd 200:27–31
35. Juneja JM, Tyagi AK, Chattopadhyay G, Seetharaman S (1995) Sub-solidus phase equilibria in the NdF_3-Nd_2O_3 system. Mater Res Bull 20:1153–1160
36. Kozak Ad, Samouel M, Erb A (1980) Le system DyF_3-Dy_2O_3. Rev Chim Miner 17:440–444